# Data-true Characterization Of Neuronal Models

2011

Jose Suarez
*University of Central Florida*

# Data-True Characterization of Neuronal Models

by

Jose Suarez
B.S. Univ. of Central Florida, 2009

A thesis submitted in partial fulfillment of the requirements
for the degree of Master of Science
in the Department of Electrical Engineering and Computer Science
in the College of Engineering and Computer Science
at the University of Central Florida
Orlando, Florida

Summer Term
2011

Major Professor: Aman Behal

# ABSTRACT

In this thesis, a weighted least squares approach is initially presented to estimate the parameters of an adaptive quadratic neuronal model. By casting the discontinuities in the state variables at the spiking instants as an impulse train driving the system dynamics, the neuronal output is represented as a linearly parameterized model that depends on filtered versions of the input current and the output voltage at the cell membrane. A prediction error-based weighted least squares method is formulated for the model. This method allows for rapid estimation of model parameters under a persistently exciting input current injection. Simulation results show the feasibility of this approach to predict multiple neuronal firing patterns. Results of the method using data from a detailed ion-channel based model showed issues that served as the basis for the more robust resonate-and-fire model presented.

A second method is proposed to overcome some of the issues found in the adaptive quadratic model presented. The original quadratic model is replaced by a linear resonate-and-fire model -with stochastic threshold- that is both computational efficient and suitable for larger network simulations. The parameter estimation method presented here consists of different stages where the set of parameters is divided in to two. The first set of parameters is assumed to represent the subthreshold dynamics of the model, and it is estimated using a nonlinear least squares algorithm, while the second set is associated with the threshold and

reset parameters as its estimated using maximum likelihood formulations. The validity of the estimation method is then tested using detailed Hodgkin-Huxley model data as well as experimental voltage recordings from rat motoneurons.

# TABLE OF CONTENTS

# LIST OF FIGURES

# CHAPTER 1

# INTRODUCTION

A fundamental issue in computational neuroscience is to characterize the relationship between the neural output recording and the input current to the cell [1], and for this reason many biologically feasible models have been proposed in literature. Spiking neural models have been extensively reasearched during the last few years, and many such models have been proposed that are highly accurate in representing the dynamics of spiking neurons. A detailed Hodgkin-Huxley model for one, can reproduce almost all types of firing patters in spiking cells, but it has one mayor drawback. Due to the fact that such a model has hundreds of parameters, it is highly inefficient to fit said parameters to experimental data. The high cost in efficieny caused by the highly detailed dynamics of the model also limits the number of cells that can be simulated in a network [2]. To overcome the defficiencies of the Hodgkin-Huxley model, many simpler models have been proposed, such as the Integrate-and-Fire (IF) model that is often used in cases where high computational efficiency is needed [3]. However, the IF model has its own issues. Because of the oversimplified nature of the model, which only has one variable, it cannot reproduce various firing patters, *e.g.*, bursting [4]. In [2], an additional variable is employed to capture the adaptation by accounting for the activation of

$K^+$ and inactivation of $Na^+$ ionic currents. This model's ability to qualitatively reproduce major firing patterns while remaining computationally efficient [5] is shown in [4, 6].

In order to fit experimental data to a particular neuronal model, selecting the right parameter estimation method is of key importance. Generally speaking, there are two base approaches to estimate the model parameters, hand tuning or computerized estimation [7]. When using the first approach, hand tuning, the model can be manually tuned to reproduce the desired biological behavior, such as in [8], where an adaptive exponential IF neuronal model is tuned to fit a detailed Hodgkin-Huxley model by hand tuning each parameter individually. Although this approach shows good results in this case, the successful implementation of such trial-and-error approach highly depends on the expertise of the researcher hand tuning the parameters and is thus labor intensive and probably inefficient when compared to an automated approach. As a results of this, it is clear to see that automated parameter estimation methods are necessary because it is unrealistic to process all the data comparisons by manual procedures [9]. In [10], a number of automated methods are discussed, including conjugate gradient, simulated annealing, and stochastic search amongst others. However these methods require large numbers of evaluations of the model, which carries a high computational cost. In [11], a database of single-compartment model neurons was constructed by exploring the entire parameter space, something that is only feasible when such a space has low dimensions. In [12], a compartment model was enhanced by using simulated annealing, a technique that will be ultimately used here, to estimate the model's parameters. A series of estimation methods for both stochastic and deterministic IF

models were presented in [1, 13, 14]. In [15], an expression for the probability distribution of a leaky integrate-and-fire (LIF) model was derived and a maximum likelihood estimate (MLE) of the input information for a LIF neuron from a set of recorded spike trains was developed.

Motivated by the computational efficiency and versatility of the adaptive quadratic model presented in [2], an estimation method is proposed in Chapter 2 to automatically estimate the parameters of the model using both input and ouput reference data. The neuronal output can be represented as a linear in the parameters (unknown parameters) model by casting the discontinuities in the state variables at the spiking instants as an impulse driving the system dynamics. Such model will depend on filtered versions of the input and output data. Furthermore, the idea of persistent excitation is used to design input signals that are able to generate rich excitation in the model such that an adequately weighted least squares based approach drives the parameter estimation errors to asymptotically converge to zero even under the presence of measurement noise.

An assumption made in the model of [2] prevented the approach proposed in Chapter 2 from being applicable to arbitrary experimental data. While the quadratic model is known to be able to reproduce biologically meaningful firing patterns, it can only reproduce these patterns qualitatively, not quantitatively – specifically, the model cannot quantitatively reproduce the upstroke/downstroke of the spike unless the parameters are assumed to be voltage-dependent [5]. Since the main interest is only in reproducing a spiking pattern and not the shape of the spike itself, a method is proposed in Chapter 3, where the

spike shape-related quadratic term was dropped so that the resulting 'resonate-and-fire' model only described the subthreshold dynamics of the system. This made it possible to narrow down the interest zone to the now-linear subthreshold region, thus making the upstroke/downstroke irrelevant to the identification of the system. Furthermore, the resulting linearity of the subthreshold model allowed for it to be treated analytically, which was useful for deriving closed form solutions and computing the update law. However, an additional challenge introduced was the requirement for separate estimation of the threshold and the post-spike reset parameters.

Here, the unknown threshold of the resonate-and-fire model is considered to be a stochastic variable. By considering the threshold to be the only stochastic component, the membrane potential at subthreshold levels is thus deterministic and solvable from which an estimate of the subthreshold parameters can be made. Under the assumption that both the input to the cell and the resulting membrane potential trace are known for characterization, the parameters for the subthreshold dynamics are estimated using a nonlinear least squares approach while the parameters associated with the threshold distribution as well as the post-spike reset of the state variables are estimated using simulated annealing to maximize the likelihood of the observed spiking pattern. Simulation and experimental results using *in-vitro* motoneuron data show that the two stage estimation process is able to find a set of parameters for the resonate-and-fire model such that there is a good match between the target and predicted spike patterns.

The remainder of this document is organized as follows. In Chapter 2, the adaptive quadratic model is presented and the following are discussed on different sections within the chapter: problem statement, technical details, identification procedure, and the results of the simulations and the use of experimental data. The maximum likelihood estimator for the stochastic resonate-and-fire neuronal model is discussed in Chapter 3. Appropriately, conclusions for the work presented are drawn and discussed in Chapter 4.

# CHAPTER 2

# WEIGHTED LEAST SQUARES

## 2.1 Problem Formulation

A simple adaptive quadratic spiking model can be described by the state equations [2]

$$\frac{dv}{dt} = k_1 v^2 + k_2 v + k_3 - k_4 (u - i) \tag{2.1}$$

$$\frac{du}{dt} = a(bv - u) \tag{2.2}$$

and the post-spike resetting

$$if\ v = V_p,\ then \begin{cases} v \to c \\ \\ u \to u + d \end{cases}. \tag{2.3}$$

Here, $v$ denotes the membrane potential and is the only system output, $u$ is a membrane recovery state variable which provides a negative feedback to $v$, while $i$ denotes injected current and/or synaptic current. At the peak $V_p$ of the membrane potential, the state variables are reset according to (2.3) – here, $c$ denotes the post-spike reset value of the membrane potential while $d$ denotes the amount of spike adaptation of the recovery variable. The parameters $k_4$ and $a$ denote the time scale of the two state variables, the parameter $b$

is the level of subthreshold adaptation, while the parameters $k_1$, $k_2$, and $k_3$ are linked to the spike initiation behavior of the neuron.

The peak membrane potential $V_p$ is directly observable from experimental data, thus, it is considered to be known. However, the remaining set of eight parameters denoted by $\theta_o = (k_1, k_2, k_3, k_4, a, b, c, d)$ is considered to be unknown. The goal is to estimate these parameters such that the spiking pattern of the quadratic spiking model with the estimated parameters can replicate (a) the spiking pattern of the exact-knowledge model (2.1)–(2.3), (b) the spiking pattern of the exact-knowledge model (2.1)–(2.3) under measurement noise, and (c) the firing pattern of a Hodgkin-Huxley type detailed reference model; specifically, a model of a spiking pyramidal cell with voltage-dependent currents [17] with parameter values used in [18] (code for this model available at [19]).

## 2.2 Technical Details

### 2.2.1 Discontinuities at Spike Times

Motivated by the desire to utilize a prediction error based automatic estimation method, we first integrate the discontinuities given by (2.3) into the state equations of (2.1) and (2.2). Since the resetting of the membrane potential in (2.3) always happens at the time when $v$ equals to the peak value $V_p$, the resetting can be considered as a jump with interval of $c - V_p$,

which can be modeled as a step input as follows

$$v \rightarrow v + (c - V_p)s(t - t_{s_j}) \tag{2.4}$$

where $s(t - t_{s_j})$ denotes a unit step at the occurrence of the $j^{th}$ spike at time $t_{s_j}$. By taking the time derivative of (2.4), and combining with (2.1), one obtains

$$\frac{dv}{dt} = k_1 v^2 + k_2 v + k_3 - k_4 (u - i) + (c - V_p)\delta(t - t_{s_j}) \tag{2.5}$$

where $\delta(t - t_{s_j})$ denotes a unit impulse at time $t_{s_j}$. Note that (2.5) correctly represents the $v$ dynamics $\forall\ t_{s_{j-1}} < t < t_{s_{j+1}}$. It is easy to see that the $v$ dynamics valid over all spiking instants can be obtained by introducing a train of impulses into the dynamics as follows

$$\frac{dv}{dt} = k_1 v^2 + k_2 v + k_3 - k_4 (u - i) + (c - V_p) \sum_j \delta(t - t_{s_j}). \tag{2.6}$$

Similarly, the discontinuity in $u$ at a spike instant $t_{s_j}$ can also be modeled as a step input as follows

$$u \rightarrow u + ds(t - t_{s_j}). \tag{2.7}$$

Following arguments similar to those made above, the $u$ dynamics valid over all spiking instants can be compactly described in the following manner

$$\frac{du}{dt} = -au + abv + d \sum_j \delta(t - t_{s_j}) \tag{2.8}$$

where (2.2) and (2.7) have been utilized. Thus, the dynamics of (2.1)–(2.3) have been compactly recast into the dynamics of (2.6) and (2.8) – a form that is amenable to linear parameterized (LP) model development.

### 2.2.2 LP Model Development

By substituting the Laplace transformation of (2.8) into that of (2.6) and conveniently re-arranging terms, one can obtain

$$\begin{aligned} s(s+a)V = \; & k_1(s+a)L(v^2) + k_2(s+a)V \\ & + \frac{k_3 a}{s} - k_4 abV + k_4(s+a)I \\ & + (s+a)[v(0) + (c - V_p)\sum_j \exp(-st_{s_j})] \\ & + k_3 - k_4 u(0) - k_4 d \sum_j \exp(-st_{s_j}) \end{aligned} \tag{2.9}$$

where $L(\cdot)$ denotes the Laplace operator, $s$ denotes the Laplace variable, $V$ and $I$ are are the Laplace transform of $v$ and $i$, respectively. In order to develop a model that is independent of the derivatives of the input and the output, a low pass filter of the form [20]

$$\frac{1}{A} = \frac{1}{s^2 + \beta_1 s + \beta_0} \tag{2.10}$$

is applied to the dynamics represented by (2.9). After conveniently rearranging terms, one can obtain

$$\begin{aligned} V = \; & \frac{k_1(s+a)L(V^2)}{A} \\ & + \frac{[(k_2 + \beta_1 - a)s + k_2 a + \beta_0 - k_4 ab]V}{A} \\ & + \frac{k_4(s+a)I}{A} \\ & + \frac{[(c - V_p)(s+a) - k_4 d]\sum_j \exp(-st_{s_j})}{A} \\ & + \frac{(s+a)v(0)}{A} + \frac{k_3}{A} - \frac{k_4 u(0)}{A}. \end{aligned} \tag{2.11}$$

It is clear to see that the last row of (2.11) denotes signals that do not persist beyond an initial transient and hence can be excluded from further analysis. By a slight abuse

of notion (specifically, the use of mixed notation), a compact representation for a linearly parameterized realizable model is obtained as follows

$$v = W\left(v, i, t_{s_j}\right)\theta \tag{2.12}$$

where $W\left(v, i, t_{s_j}\right) \in \Re^{1\times 9}$ is a realizable regression vector which is defined as follows

$$\begin{aligned} W = \quad & \left[\frac{s}{A}L(v^2), \frac{1}{A}L(v^2), \frac{s}{A}V, \frac{1}{A}V, \frac{1}{sA}, \frac{s}{A}I, \frac{1}{A}I, \right. \\ & \left. \frac{s}{A}\sum_j \exp(-st_{s_j}), \frac{1}{A}\sum_j \exp(-st_{s_j})\right] \end{aligned} \tag{2.13}$$

while $\theta \in \Re^9$ is an unknown parameter vector which is defined as follows

$$\begin{aligned} \theta = \quad & [k_1,\ k_1 a, k_2 + \beta_1 - a, k_2 a + \beta_0 - k_4 ab, \\ & k_3 a, k_4, k_4 a, c - V_p, a(c - V_p) - k_4 d]^T . \end{aligned} \tag{2.14}$$

Note that the derived parameter vector $\theta$ is an over-parameterized (by 1) function of the original parameter set $\theta_o$.

### 2.2.3 Weighted Least Squares Algorithm

Based on the LP model derived above in (2.12), a prediction error based estimation algorithm can be developed. Although a gradient-based law is known to achieve a greater rate of convergence, it is highly sensitive to measurement noise. However, estimation based on least squares is robust to presence of noise and thus is considered for implementation. The instantaneous prediction error is defined as follows

$$e = \hat{v} - v = W(\cdot)\hat{\theta} - v \tag{2.15}$$

where $\hat{v} = W(\cdot)\hat{\theta}$ denotes the predicted output. A standard objective function for least squares estimation is given as follows

$$J = \int_0^t e^2(r)dr = \int_0^t \left\| v(r) - W(r)\hat{\theta}(t) \right\|^2 dr. \tag{2.16}$$

It is important to consider the fact that the objective here is to estimate parameters such that the spiking pattern of a neuron can be reproduced by the proposed model – thus, the behavior of the neuron around the time of spike initiation is much more important than its behavior at all other times. However, since the contribution of spike in the above objective function $J$ is rather small due to its short interval of occurrence compared with the time of occurrence of pre- and post-spiking activity, the objective function above needs to be weighted appropriately in order to achieve the research objective. Thus, the objective function is redefined as follows

$$J = \int_0^t k(r)e^2(r)dr = \int_0^t k(r) \left\| v(r) - W(r)\hat{\theta}(t) \right\|^2 dr \tag{2.17}$$

where $k(t)$ denotes a weight term which can be chosen to be larger during spike occurrence. After taking the derivative of the objective function of (2.17), we obtain

$$\frac{dJ}{d\hat{\theta}} = -2\int_0^t k(r)W^T(r)[v(r) - W(r)\hat{\theta}(t)]dr. \tag{2.18}$$

When the objective function is minimized, one can obtain

$$\int_0^t k(r)W^T(r)W(r)dr\hat{\theta}(t) = \int_0^t k(r)W^T(r)v(r)dr.$$

By defining

$$P = \left[\int_0^t k(r)W^T(r)W(r)dr\right]^{-1}, \tag{2.19}$$

one can easily obtain the dynamics for parameter estimation as follows

$$\dot{\hat{\theta}} = -k(t)P(t)W^T(t)e \tag{2.20}$$

$$\dot{P} = -k(t)PW^T(t)W(t)P. \tag{2.21}$$

By solving (2.19), (2.20) and (2.21), one can easily show that

$$\tilde{\theta}(t) = P(t)P^{-1}(0)\tilde{\theta}(0) \tag{2.22}$$

where $\tilde{\theta} = \hat{\theta} - \theta \in \Re^9$ denotes the parameter estimation error. It is well known that the estimated parameters will asymptotically converge to the true parameters, *i.e.,* $\lim_{t\to\infty} \tilde{\theta}(t) = 0$ as long as $W(\cdot)$ is persistently exciting [20].

## 2.3 Procedure

### 2.3.1 Reference Data Generation

Three types of reference data are generated for use during system identification. The first type of reference data is output data from the adaptive quadratic model itself. This is used to test the validity of the approach as well as the capability to replicate several types of biologically relevant firing patterns. In the second set of reference data, measurement noise is considered, which is common in biological systems – this is used to test the robustness of the proposed approach. The last type of reference data is output data from the detailed ion-channel based spiking model (Hodgkin-Huxley model) of [17] with parameters from [18].

For asymptotic convergence of the parameter estimation error, the injected current input $i$ needs to be properly designed in order to ensure the persistent excitation of the regression matrix $W(\cdot)$ of (2.13). Given the fact that a reference containing a single sinusoidal frequency can be utilized to estimate two parameters for linear system dynamics [20], a combination of sinusoids at four different frequencies has been utilized to estimate the parameter vector $\theta \in \Re^9$ of (2.14) – here, the fact that the square nonlinearity in the output generates extra excitation in the system is being utilized. Specifically, the waveform type employed for generating the input $i$ is given as follows

$$i = I_1 \sin(\omega_1 t) + I_2 \sin(\omega_2 t) + I_3 \sin(\omega_3 t) + I_4 \sin(\omega_4 t) \tag{2.23}$$

where $I_i$ and $\omega_i \ \forall \ i = 1, 2, 3, 4$, respectively, denote the amplitudes and frequencies of the underlying sinusoids.

### 2.3.2 Parameter Estimation

Given the reference data generated through (2.23) and the recorded output $v$, the data is processed to determine $V_p$, the spike instants $t_{s_j}$, and the corresponding impulse train. To obtain the regression vector (2.13), the parameters for the low-pass filter (2.10) need to be selected. The cutoff frequency of the low-pass filter is lower-bounded by the highest frequency of the input current and is upper-bounded by the measurement noise in the system. Based

on the aforementioned choices, the estimation algorithm is implemented according to (2.15), (2.20), and (2.21).

After estimation, the original parameters $\theta_o = (k_1, k_2, k_3, k_{4,}a, b, c, d)$ need to be retrieved from the estimated derived parameter vector $\hat{\theta}$. According to (2.14), the relationship between the original parameter and derived parameter $\theta$ can be represented as a nonlinear function $\theta = \theta(\theta_o)$. A nonlinear optimization algorithm (*e.g.,* nonlinear optimization toolbox in *MATLAB*) can be utilized to select the best value for $\theta_o$ that minimizes the difference between $\theta(\theta_o)$ and estimated $\hat{\theta}$. Finally, to evaluate the validity of the estimated model parameters, either step or periodic input currents are utilized to compare membrane voltage data from actual and estimated system models.

## 2.4 Results and Discussion

The simulation of the quadratic model is run in *MATLAB/SIMULINK* environment while the detailed model of the cell is run in the *NEURON* environment [21]. All estimation code is run in *MATLAB/SIMULINK*. The low pass filter parameters defined in (2.10) are chosen as $\beta_1 = 2$ and $\beta_0 = 1$. In what follows, the results obtained from the three types of reference data previously described are discussed in detail.

### 2.4.1 Results for Quadratic Reference Data

To generate this type of reference data, the injected current (2.23) is chosen as follows

$$I_1 = 3.9 \qquad I_2 = 13 \qquad I_3 = 9.1 \qquad I_4 = 15.6$$

$$\omega_1 = 0.5 \qquad \omega_2 = 2.25 \qquad \omega_3 = 2.0 \qquad \omega_4 = 2.5$$

where the currents have the units of $pA$ while the frequencies are expressed in $rad \cdot ms^{-1}$. Given this reference input signal, various sets of model parameters are utilized from [4] to generate corresponding membrane potential output waveforms. First, a rapidly adapting receptor is simulated (*i.e.,* receptor initially fires and then quickly stops firing in response to steady input) using the following set of parameters from [4]

$$\theta_o = (0.04, 5, 140, 1, 0.02, 0.2, -65, -0.5).$$

Fig. 2.1 (a) shows the output of the exact model to the injected reference sinusoidal input current with parameters described above. Fig.2.1 (b) shows the parameter estimation errors (only two sample parameter estimates are presented here) which rapidly converge toward zero. Specifically, the parameter estimation converges towards its true value quickly and then shows tiny oscillations around its true value. The estimation is run much longer after the errors are under 5% to ensure enough data points exist to exactly retrieve the original parameters $\theta_o$. The estimate of $v$ is shown in Fig. 2.1 (c). From Figs. 2.1 (a) and (c), the convergence of the prediction error can be clearly seen. To validate the effectiveness of the system identification, a step current $i = 3.5pA$ is applied to the exact and the estimated quadratic models. Fig. 2.2 shows that the prediction achieves the expected rapid adaptation

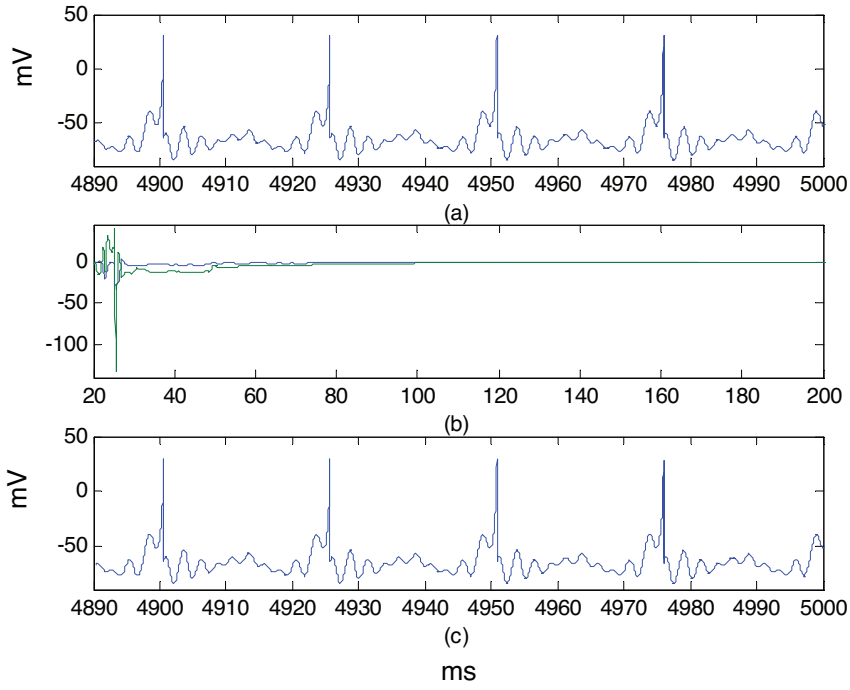


Figure 2.1: (A) Reference data used to identify the parameter of the quickly-adapting receptor. (B) Rapid convergence of of estimation error (in percentage) of two sample parameters is shown. The least squares algorithm does not apply until $20ms$, when the impact of the initial conditions in (2.9) goes to 0. (C) Estimated behavior from identification mechanism.

behavior of the exact model; in fact, prediction exactly locates the first three spikes. Fig. 2.3 shows the most common type of excitatory neuron in mammalian neocortex which fires with decreasing frequency. The following parameters were utilized

$$\theta_o = (0.04, 5, 140, 1, 0.01, 0.2, -65, 8)$$

to generate the reference data in such a type of pattern and a step input current $i = 30pA$ was injected to evaluate the efficacy of the identification. The result shows that the prediction

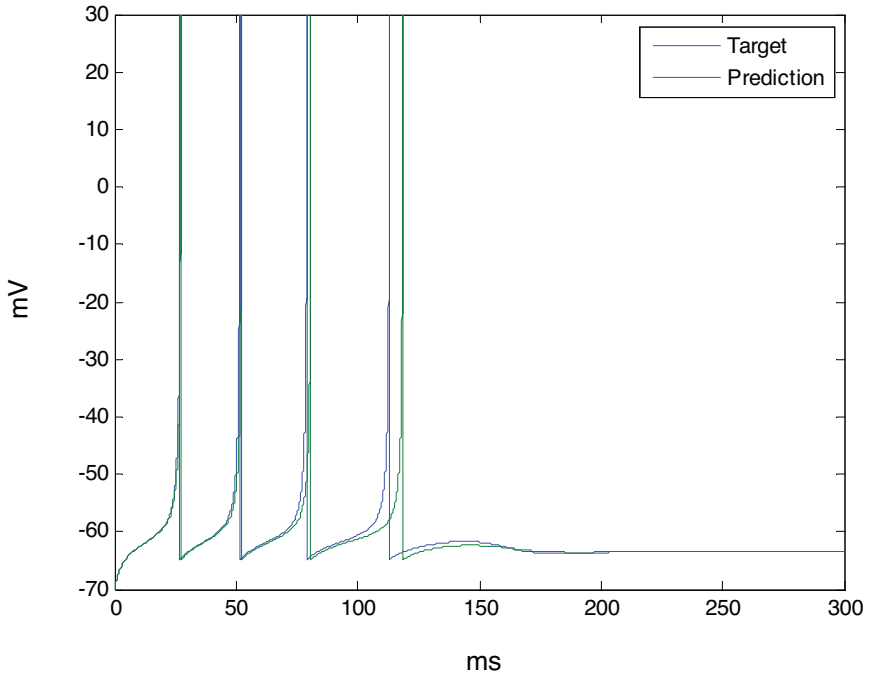


Figure 2.2: Voltage trace of prediction and target data for a rapidl adapting neuron. Both subthreshold traces and spikes are superimposed at the beginning.

curve almost exactly follows the target data initially but over-adapts gradually. Another important firing pattern is tonic bursting as shown in Fig. 2.4, which can be found in the chattering neurons in the cat neocortex [22]. To generate the reference data for identification, the model parameters are chosen as follows

$$\theta_o = (0.04, 5, 140, 1, 0.02, 0.2, -50, 2).$$

For validation, injected currents were chosen to be $i = 15pA$. The prediction in the Figs. 2.4 shows a phase shift compared with the target data. However, the result is still successful in

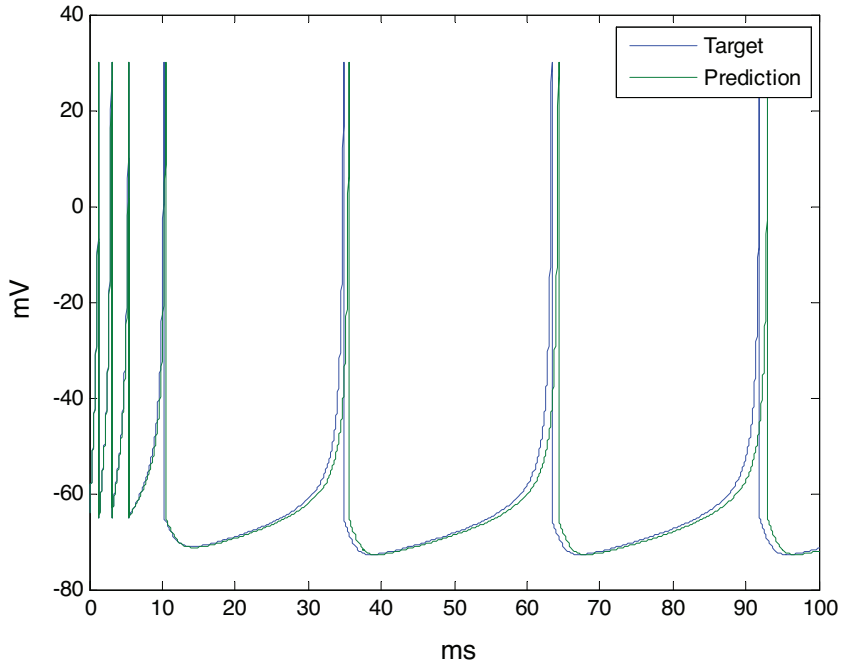


Figure 2.3: Target and predicted voltage traces of a neuron firing with decreasing frequency. The prediction follows the spike frequency adaptation behavior, but shows over adaptation. following the pattern of target data, thus the information encoded in the inter-spike frequency is not lost.

### 2.4.2 Results for Noisy Quadratic Reference Data

When generating this type of reference data, the injected current is chosen identical to Section 2.4.1. To simulate measurement noise, the reference membrane potential data obtained are corrupted by adding white noise with a signal-to-noise ratio of $40dB$. Results are shown in

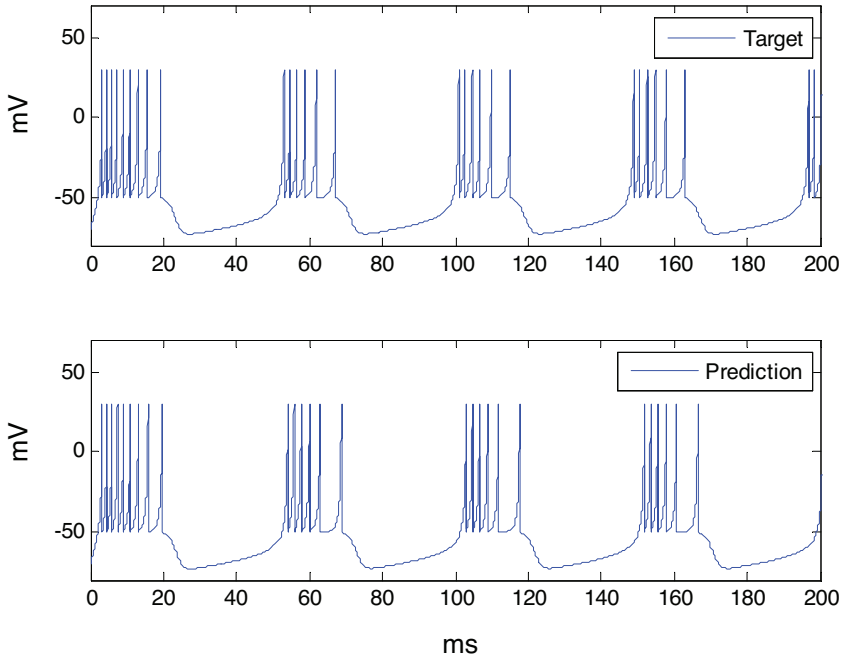


Figure 2.4: Target and Predicted spike trains. The prediction replicates the firing patten (tonic bursting) with a small constant delay with respect to the target data.

Fig. 2.5 - 2.6. In Fig. 2.5, results for estimates of two sample parameters are shown. It can be seen that one of the parameters converges quickly while the other one shows some oscillation about its true value on account of noise in the measurement – however, such oscillations can be accounted for through an averaging process during retrieval of the original parameters via the nonlinear optimization procedure discussed in the previous section. Fig. 2.6 shows a tonic spiking pattern obtained by using

$$\theta_o = (0.04\ 5\ 140\ 1\ 0.02\ 0.2\ \ -65\ 2)$$

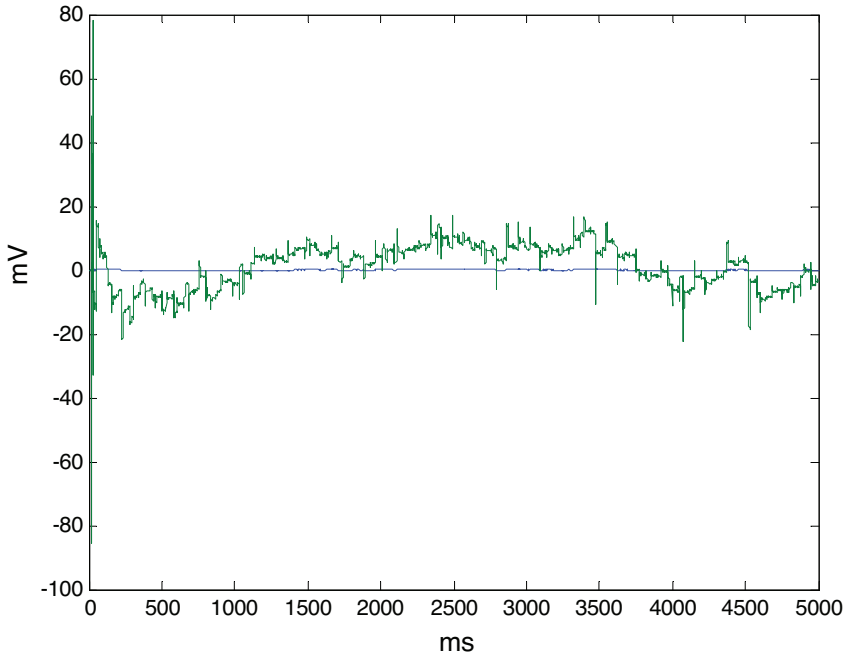


Figure 2.5: The estimation error (in percentage) of two parameters under noisy reference data.

to generate the reference data. To validate the identification, a step input of $i = 12pA$ is injected. While Fig. 2.6 shows a slight amount of under-adaptation, it can be concluded that the proposed approach is robust to the presence of noise.

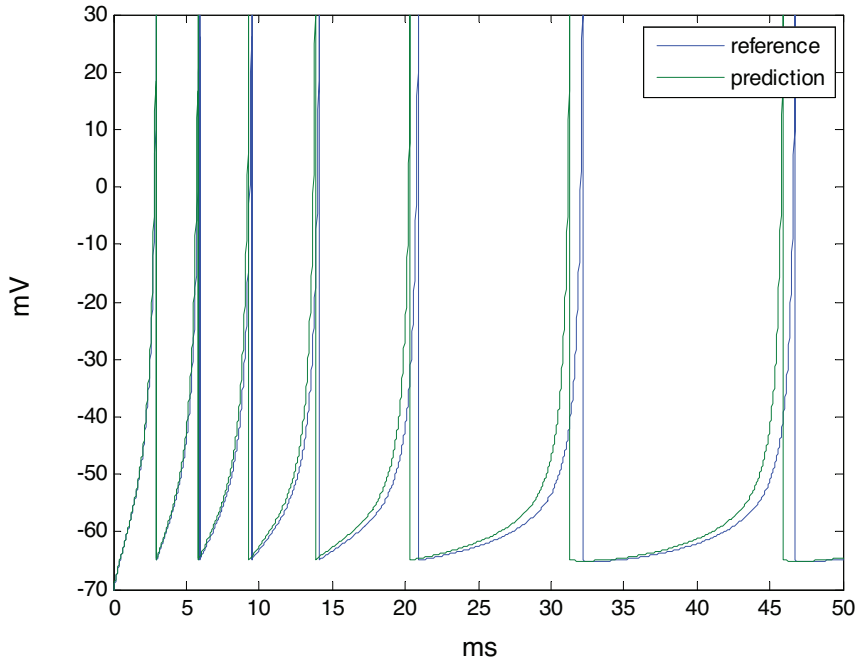


Figure 2.6: Voltage trace of prediction and target data under step input. Prediction shows under adaptation.

### 2.4.3 Results for Detailed (Hodgkin-Huxley) Model Data

The injected current for generating this type of reference data is chosen as follows

$$I_1 = 0.21 \qquad I_2 = 0.7 \qquad I_3 = 0.49 \qquad I_4 = 0.84$$

$$\omega_1 = 0.1 \qquad \omega_2 = 0.45 \qquad \omega_3 = 0.4 \qquad \omega_4 = 0.5$$

where the currents have the units of $pA$ while the frequencies are expressed in $rad \cdot ms^{-1}$. The weight term $k$ is chosen to be 2 during the upstroke of the spike and 1 everywhere else, thereby, weighting the instantaneous error higher during the upstroke of the spike than elsewhere in the voltage trace. Under periodic input of the type given by (2.23), the match

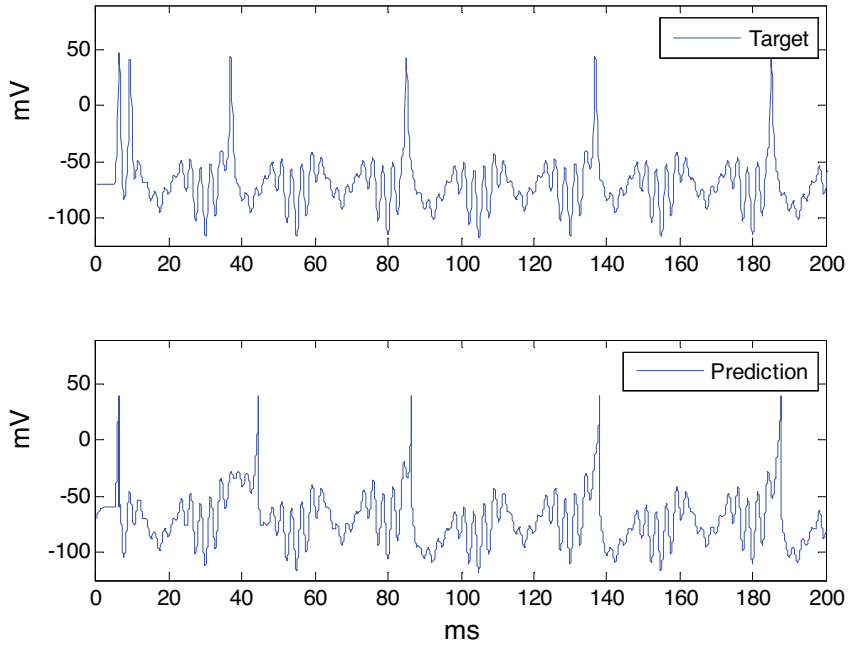


Figure 2.7: Spike trains of prediction and target data from detailed (Hodgkin-Huxley type) regular spiking model. Spikes from the two trains have similar firing rates.

between adaptive quadratic model and detailed regular spiking model is shown in Fig 2.7. Although the prediction misses one spike at the beginning, the firing rates between the prediction and the reference are close. However, replicating the experimental behavior with the estimated parameters under a step input was not possible. This issue is discussed at length in Chapter 4.

### 2.4.4 Comparison with Existing Techniques

In this section, we compare the result from the proposed method with an existing estimation technique, *e.g.*, the CAPTAIN Toolbox [23] which consists of several Matlab functions for system identification. Since the LP model (2.12) is linear in parameters, function dlr (Dynamic Linear Regression) is employed to identify the parameters, given the same reference data as used in Section 2.4.1. The evaluation result is shown in Fig. 2.8. Comparing with Fig. 2.3, one will find that the proposed method outperforms the CAPTAIN in that the prediction as shown in Fig. 2.3 is tighter than in Fig. 2.8. Finally, we note here that we were unable to compare the proposed approach with functions from the CONTSID toolbox [24] (also available in Matlab) because CONTSID is only applicable to linear models while the model given by (2.1)–(2.3) (or the equivalent model given by (2.6) and (2.8)) is clearly nonlinear because of the square nonlinearity associated with the output voltage.

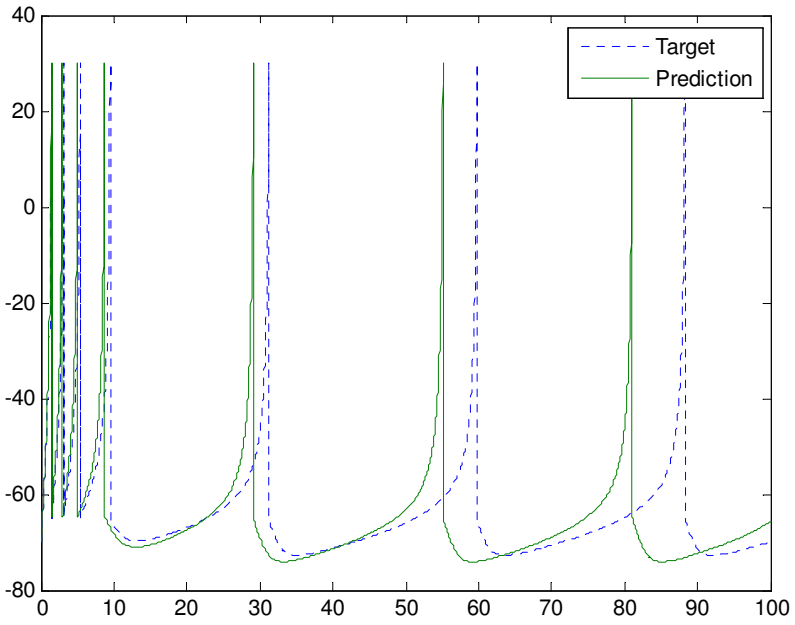


Figure 2.8: Results obtained from the CAPTAIN toolbox.

# CHAPTER 3

# TWO-STAGE ESTIMATION STRATEGY

## 3.1 System Model

A resonate-and-fire neuronal spiking model can be described by the state equations [30]

$$\frac{dv}{dt} = k_1 v + k_2 - k_3 u + k_3 i \tag{3.1}$$

$$\frac{du}{dt} = a(bu - v) \tag{3.2}$$

where $v$ denotes the membrane potential and is the only system output, $u$ is an immeasurable membrane recovery state variable which provides a negative feedback to $v$, while $i$ denotes injected current and/or synaptic current. The parameters $k_3$ and $a$ denote the time scale of the two state variables, the parameter $b$ is the level of subthreshold adaptation, while the parameters $k_1$ and $k_2$ are linked to the subthreshold behavior of the neuron. When the membrane potential $v$ hits the threshold, the neuron is said to fire a spike, and the state variables are reset according to

$$\text{if } v = V_t, \text{ then } \begin{cases} v \to c \\ \\ u \to u + d \end{cases} \tag{3.3}$$

where $V_t$ is the threshold, $c$ denotes the post-spike reset value of the membrane potential, while $d$ denotes the amount of spike adaptation of the recovery variable. Note that the post threshold dynamics of the cell are not described by the model of (3.1) and (3.2); these equations only describe the subthreshold behavior. Unlike the triangular pulse used by [31] to mimic the shape of the spike, here the entire spiking behavior is ignored, using only a straight line to indicate the occurrence of a spike.

Since the model above is only valid in the subthreshold region, a voltage threshold needs to be defined to indicate the initiation of a spike. A fixed threshold is used by [30]. However, empirical evidence suggests that the voltage threshold for a spike depends not only on the instantaneous value of the voltage, but also on the rate of voltage change. The variation in the spike threshold could also be a function of the instantaneous firing rate [32]. Using a detailed ion-channel based spiking model [17] with parameters by [18], the probability of firing as a function of membrane potential [33] was used to identify a specific value that could be considered as a fixed threshold, but no such value could be clearly identified, i.e., we could not determine an obvious "jump point" in firing probability which can be defined as a "threshold". Thus, there is an indication that a more realistic model should consider a threshold distribution rather than a deterministic value. Stochastic spike thresholds have been previously proposed and proved [34, 35]. Others have used a stochastic term in the membrane dynamics to represent signal noise, e.g., see [14]. In fact this is computationally identical to subtracting the noise from the potential and adding it to the threshold [36]. The

threshold is considered to be a random variable and its distribution is assumed to be i.i.d. and Gaussian, *i.e.*, $V_t \sim N(m, \sigma)$.

## 3.2 The Estimation Problem

The goal is to estimate the following set of unknown parameters associated with the resonate-and-fire neuron model

$$\theta \triangleq (k_1, k_2, k_3, a, b, c, d, m, \sigma) = (\theta_l, \theta_t)$$

where the partitions $\theta_l$ and $\theta_t$ will be explicitly defined below. It is assumed that the input excitation and membrane potential depolarization recordings are available for measurement. Given the membrane potential trace, it is possible to obtain the spike locations and infer the inter-spike intervals (ISIs). Given the model of (3.1)-(3.3), the system parameters to be estimated are divided into two sets; specifically, a set

$$\theta_l \triangleq (k_1, k_2, k_3, a, b)$$

which is associated with the linear dynamics of (3.1) and (3.2), and another set

$$\theta_t \triangleq (c, d, m, \sigma)$$

which is linked to the after-spike resetting and threshold distribution parameters. Thus, the two-stage estimation problem solved here consists of both matching the subthreshold voltage recording to estimate $\theta_l$ and utilizing those estimates as well as the measurements to maximize the likelihood of the observed spiking pattern to estimate $\theta_t$.

### 3.2.1 Subthreshold Estimation (Stage I)

The linear system represented by (3.1) and (3.2) can be analytically treated and solved, which is particularly useful when using gradient based or least squares based estimation techniques, since these require the derivative of the objective function with respect to the parameters. Based on (3.1) and (3.2), the solution for the subthreshold membrane potential can be expressed as

$$v\left(t\right) = \left[k_2 - k_3 u(t_0)\right] f_1(\theta_l, t) + k_3 (f_2\left(\theta_l, t\right) * i) + v(t_0) f_2(\theta_l, t) + k_2 a f_3(\theta_l, t) \tag{3.4}$$

where where $u\left(t_0\right)$ and $v\left(t_0\right)$ are initial values for $u$ and $v$, the symbol $*$ denotes the convolution operator, while the functions $f_1\left(\theta_l, t\right)$, $f_2\left(\theta_l, t\right)$, and $f_3\left(\theta_l, t\right)$ in the solution have explicitly been defined in Appendix A. Because of the dependence of $v\left(t\right)$ on $u\left(t_0\right)$ and $v\left(t_0\right)$ as can be seen in (3.4), $v\left(t\right)$ depends not only on the parameter set $\theta_l$ but also on the reset values $c$ and $d$. However, at this stage, the effect of $c$ and $d$ is set aside by utilizing a spike-free continuous subsequence of the measured data that lies beyond an initial transient period; functionally, this is equivalent to setting $u(t_0) = v\left(t_0\right) = 0$ in (3.4). This results in voltage dynamics that are independent of $\theta_t$ in the subthreshold region, depending only on $\theta_l$ such that $v\left(t\right)$ can be compactly expressed as $v = f(t, i, \theta_l)$. Given input $i$, $f$ is a nonlinear function on the parameter set $\theta_l$. The estimate for $\theta_l$ is made via a nonlinear least squares estimation based technique by [37]. Nonlinear least squares is a form of least squares used to fit observations to a model that is nonlinear in the parameters. Given a discrete observed

data sequence of length $N$, the objective function to be minimized is

$$S = \sum_{i=1}^{N} (v_i - \hat{v}_i)^2$$

where $\hat{v}_i \triangleq f(i, t; \hat{\theta}_l)$ denotes the estimated voltage at time $i$. The parameter is updated using the following iterative scheme

$$\hat{\theta}_l^{t+1} = \hat{\theta}_l^t + J'^{-1} J' \Delta v \tag{3.5}$$

where $\Delta v = v - \hat{v}$ is a $n \times 1$ vector defining the error between the measured and the estimated voltage while $J$ is the $N \times M$ Jacobian matrix, with elements given by

$$J_{ik} = \frac{\partial \hat{v}_i}{\partial \hat{\theta}_{l_k}}. \tag{3.6}$$

Here, $M = 5$, being the number of parameters in the set $\theta_l$. Furthermore, $\hat{\theta}_{l_k}$ denotes the estimate of the $k^{th}$ element of the parameter vector $\theta_l$. Note that the Jacobian matrix $J$ is a function of the estimated parameters and updates from one iteration to the next. The convergence of the parameter estimates to their actual values is ensured by utilizing a persistently exciting input current injection as it has been demonstrated in earlier work [16].

### 3.2.2 Threshold Distribution and Reset Parameters Estimation (Stage II)

#### 3.2.2.1 Strategy

During this stage, the subthreshold parameters $\hat{\theta}_l$ estimated from the previous step are utilized in the reconstruction of the subthreshold membrane potential. Based on (3.4), we

can explicitly write the dependencies of the reconstructed potential $\hat{v}(\cdot)$ as follows

$$\hat{v} = g\left(t, i, \hat{\theta}_l, c, d\right). \tag{3.7}$$

Conditional upon $i$ and $\hat{\theta}_l$, it can be seen that $\hat{v}$ is a linear function of the unknown reset parameters $c$ and $d$. We remark that in Stage II, the reset parameters (*i.e.,* the initial conditions post spiking) cannot be ignored because these parameters strongly determine the rate of occurrence of spikes. The insight here is that the reconstructed membrane potential is allowed to evolve according to (3.7) and spikes are generated when the reconstructed membrane potential reaches threshold $V_t \sim N(m, \sigma)$; the unknown parameters $c, d, m$, and $\sigma$ are adjusted so as to maximize the likelihood of occurrence of the observed firing pattern. During this stage, it is assumed that the the only output measured from the cells is the location of the spikes. Since the spikes from real neurons have finite width, the spike time $t_j$ is defined to be the time of the peak of each spike. During the interval $t \in (t_{j-1}, t_j)$, the cell is not firing. All data points during the intervals $\bigcup_j (t_{j-1}, t_j)$ can be denoted as $t_i$, since the data being examined has been discretized. The likelihood function for the parameter set $\theta_t$ can therefore be defined as the probability that the stochastic threshold $V_t$ is below the reconstructed membrane potential $\hat{v}$ at spike times $t_j$ and above $\hat{v}$ at non-spike times $t_i$. Mathematically, the likelihood function can be expressed as follows

$$\begin{aligned} L(\theta_t) &= \log\left(\left(\prod_i \int_{\hat{v}_i}^{\infty} G(V_t; m, \sigma) dV_t\right)\left(\prod_j \int_{-\infty}^{\hat{v}_j} G(V_t; m, \sigma) dV_t\right)\right) \\ &= \sum_i \log \int_{\hat{v}_i}^{\infty} G(V_t; m, \sigma) dV_t + \sum_j \log \int_{-\infty}^{\hat{v}_j} G(V_t; m, \sigma) dV_t \end{aligned} \tag{3.8}$$

where $G(V_t; m, \sigma)$ is the Gaussian probability density function of the threshold $V_t$ with mean $m$ and variance $\sigma^2$. $L(\theta_t)$ could be referred to as "log-likelihood" as a more appropriate term,

but for simplicity reasons, it is referred to simply as "likelihood". Since $\hat{v}$ is a function of $c$ and $d$, a new voltage trace is generated using (3.7) for each set of parameters $\theta_t$. The Maximum Likelihood Estimation (MLE) parameters $\hat{\theta}_t$ are given by the maximizing argument of the likelihood function $L(\theta_t)$ of (3.8).

#### 3.2.2.2 Existence of Local Maxima

Before choosing a technique to solve (3.8), it is prudent to first study the uniqueness of the maximum of (3.8). Since the likelihood function is the log multiplication of a series of basic functions, a sufficient condition for the log concavity of the overall function of (3.8) is for each of the underlying functions to be log concave. If this condition is met, then the likelihood function has a unique maximum. To show that $\int_{-\infty}^{v_i} G\left(V_t; m, \sigma\right) dV_t$ is not log-concave, we begin by defining

$$\begin{aligned} I &= \int_{-\infty}^{v} G\left(V_t; m, \sigma\right) dV_t \\ F &= \log I \end{aligned}$$

The Hessian matrix of $F$ is

$$H = \begin{bmatrix} \dfrac{\partial^2 F}{\partial x_1^2} & \dfrac{\partial^2 F}{\partial x_1 \partial x_2} & \dfrac{\partial^2 F}{\partial x_1 \partial x_3} & \dfrac{\partial^2 F}{\partial x_1 \partial x_4} \\ \dfrac{\partial^2 F}{\partial x_2 \partial x_1} & \dfrac{\partial^2 F}{\partial x_2^2} & \dfrac{\partial^2 F}{\partial x_2 \partial x_3} & \dfrac{\partial^2 F}{\partial x_2 \partial x_4} \\ \dfrac{\partial^2 F}{\partial x_3 \partial x_1} & \dfrac{\partial^2 F}{\partial x_3 \partial x_2} & \dfrac{\partial^2 F}{\partial x_3^2} & \dfrac{\partial^2 F}{\partial x_3 \partial x_4} \\ \dfrac{\partial^2 F}{\partial x_4 \partial x_1} & \dfrac{\partial^2 F}{\partial x_4 \partial x_2} & \dfrac{\partial^2 F}{\partial x_4 \partial x_3} & \dfrac{\partial^2 F}{\partial x_4^2} \end{bmatrix}$$

where $x_i$ denotes the $i^{th}$ component of the vector $x$ which is defined as follows

$$x = \theta_t = [c, d, m, \sigma]^T .$$

The unique elements of the symmetric matrix $H$ have been explicitly defined in Appendix B. By appropriately choosing an invertible matrix $C$, we can diagonalize $H$ to obtain the matrix $D$ as follows

$$D = C^T H C = \begin{bmatrix} \left(I\frac{v-m}{\sigma^2} + G\right) & 0 & 0 & 0 \\ 0 & -1 & 0 & 0 \\ 0 & 0 & 1 & 0 \\ 0 & 0 & 0 & 0 \end{bmatrix} .$$

It is clear to see that $D$ has both positive and negative eigenvalues; thus, it is indefinite which implies that $\int_{-\infty}^{v} G\left(V_t; m, \sigma\right) dV_t$ is not log-concave. We note here that it is not essential to explicitly find the matrix $C$. In fact, the diagonal matrix $D$ was obtained through an appropriate sequence of row and column operations.

Being unable to rule out the possibility that the likelihood function has multiple local maxima, it is imprudent to utilize a method such as gradient ascent, which is very likely to get stuck at a local maximum. Therefore, we choose to utilize the simulated annealing method [38, 39] to find the maximum of the previously formulated likelihood function of (3.8).

#### 3.2.2.3 Implementation

Unlike a gradient based law which might get stuck at a local maximum, simulated annealing (SA) is designed for global optimization. This particular technique has its origin in the metallurgic industry where an annealing technique that involves the controlled heating and cooling of a material is used to minimize the energy of its crystals. After selecting an initial point, the algorithm randomly selects a point $s'$ in the neighborhood of the old point $s$ at each iteration. The newly selected point is consider or rejected as a "better" point depending on the probability function $P$, defined as

$$P = \begin{cases} 1 & \text{if } L(s') > L(s) \\ \\ e^{-1/T} & \text{otherwise} \end{cases} \tag{3.9}$$

where $T$ is denoted as the "temperature". The possibility to accept the worse point provides the algorithm the capability of getting away from the local maximum. The SA algorithm is allowed to move randomly in the entire parameter space by initializing the "temperature" with a large value $T_0$. Then the parameter gradually decreases. The "cooling" algorithm for the temperature $T$ used here is given by

$$T = T_0(1 - n/N)^2$$

where $n$ is the current iteration, and $N$ is the maximum number of iterations, after which the algorithm will stop. A detailed description of the algorithm is as follows.

- *Step 0.* Initialize the algorithm by selecting a starting point $s_o$, a starting temperature $T_o$, and a maximum number of iterations $N$. Set a boundary for each direction if needed. Then compute the likelihood for the initial point.

- *Step 1.* A new point $s'$ in the neighborhood of $s$ is generated. Projection applies if the new point exceeds the preset boundary.

- *Step 2.* The likelihood of the new point $s'$ is computed. The probability function (3.9) is called, and $s$ is replaced with $s'$ if $P$ is larger than a randomly picked up number between 0 and 1. Otherwise, $s$ remains untouched.

- *Step 3.* The current iteration $n$ is increased and the temperature $T$ is updated.

- *Step 4.* If $n < N$, go back to *Step 2*, otherwise stop the search.

## 3.3 Results and Discussion

We applied the aforementioned two-stage estimation strategy to two types of data, namely, simulated data and *in-vitro* recording from embryonic rat motoneurons. In what follows, we describe the data acquisition and processing methods and results obtained from the two types of data.

### 3.3.1 Synthetic Data

The reference data for the simulations was generated from two sources, namely, an exact resonate and fire model and a detailed Hodgkin-Huxley model. The reason for applying the method initially to reference data generated by the exact model was to validate the ability of the formulation to achieve small parameter estimation error – it is possible to do so in this case because the exact parameters are known. Next, detailed model simulation data was generated in the *NEURON* [21] simulation environment by using an ion-channel based spiking model [17] with parameters by [18]. Using the current clamp mode of the simulation, we injected pre-generated white noise current to stimulate the cell and collected membrane potential data sampled at 50Khz.

#### 3.3.1.1 Results from Exact Model Data

A parameter set for the reference model of (3.1)–(3.3) was chosen to simulate a rapidly adapting receptor (*i.e.,* receptor initially responds and then quickly stops firing in response to steady input). Fig. 3.1A shows how the estimation follows the subthreshold region of the reference data. Fig. 3.1B(top) shows the output of the exact model to an injected white noise input current stream; these input and output data streams are utilized to estimate the model parameters. The predicted output sequence generated from the estimated model under white noise injection is shown in Fig. 3.1B(bottom). It is clear to see from the two

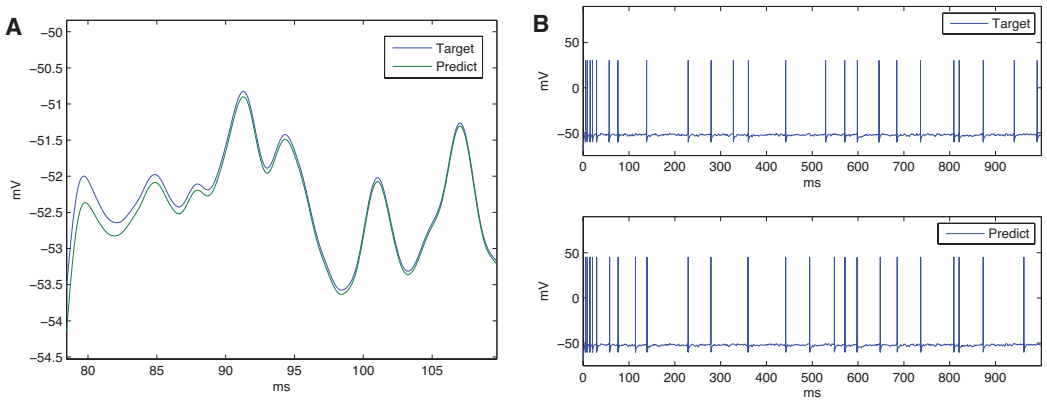


Figure 3.1: (A) The predicted subthreshold dynamics for the rapidly adapting receptor closely follow the dynamics of the reference data. (B) Comparison of spike trains. Target data is generated by white noise input to the exact model.

plots in Fig. 3.1B that the target and the predicted spiking rates track closely. In Fig. 3.2, a different spiking behavior, namely, regular-spiking, is considered by choosing an appropriate set of parameters for the model of (3.1)–(3.3). As it can be seen in Fig. 3.2A, the prediction closely follows the subthreshold region of the reference data which vouches for the success of the subthreshold estimation. Success of the Stage II estimation can be demonstrated from the results obtained from the predicted spike train, which correctly estimates the original number of spikes in the target data, as shown in Fig. 3.2B. In Fig. 3.3, a pure step input is injected to both the exact model and the estimated model to replicate the spiking behavior of a rapidly adapting receptor (Fig. 3.3A) and regular-spiking cortical neuron (Fig. 3.3B), where it can be seen in both cases that the firing pattern is correctly predicted.

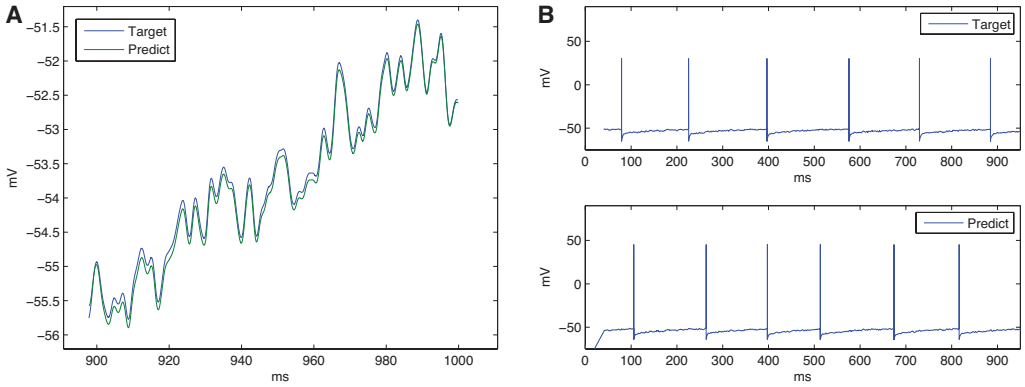


Figure 3.2: Regular-spiking Pyramidal Cell. (A) Target and predicted subthreshold dynamics. (B) Comparison of spike trains. Target data is generated by white noise input to the exact model.

#### 3.3.1.2 Results from Hodgkin-Huxley Model Data

After employing the two-stage estimation strategy using reference data generated from a detailed ion-channel based model [17] for a regular-spiking cortical cell, the ability of the estimated resonate-and-fire model to represent the detailed model data is evaluated by comparing the predicted output of the estimated model to previously unseen input data. From the subsequence of data streams shown in Fig. 3.4A, one can see that the subthreshold traces of the target and predicted data are very close, showing that dynamics (3.1) and (3.2) yield good approximations in the subthreshold region. Fig. 3.4B shows that the predicted spike trains closely follow the target with the same adaptation rate. The proposed method was evaluated 10 times. It was seen that the estimated parameters led to 14.7 spikes on

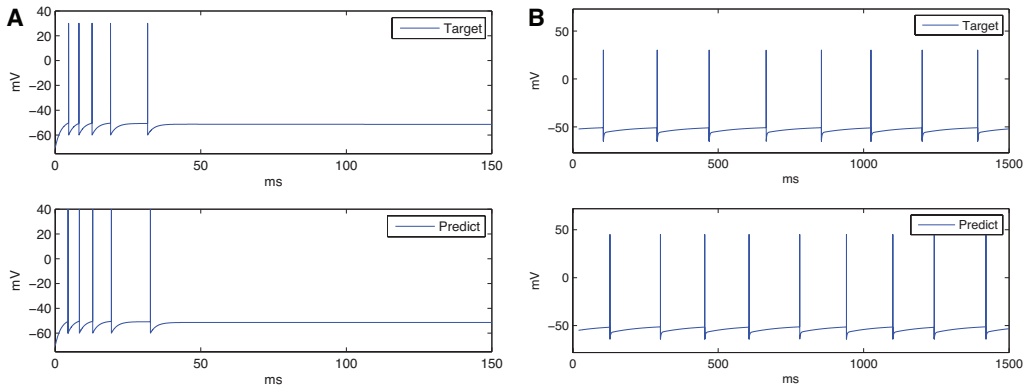


Figure 3.3: Step input response for different cells under the exact (top) and estimated (bottom) models. (A) Target and predicted spike trains for a rapidly adapting receptor, where the prediction replicates the reference firing pattern. (B) The proposed model correctly predicts the spike pattern for a regular-spiking cortical neuron.

average, while the target train had 15 spikes under the same input stimulus, thus, there was an average under-prediction of 0.3 spikes. The predicted number of spikes never deviated from the number of spikes in the reference data by more than 2 spikes during these trials. The two-stage estimation process was also applied to reference data from a fast-spiking (FS) cortical neuron generated by the previously mentioned model [17] using noisy current as the input. Fig. 3.5A shows that the estimated parameters produced by the proposed estimation process were able to generate subthreshold dynamics that closely follow the target data. Fig. 3.5B shows the reference spike train (top), and the predicted spike train (bottom), in which it can be seen that the proposed method was able to accurately replicate the number of spikes and the rate at which these occurred. 10 validation runs were utilized to quantify the accu-

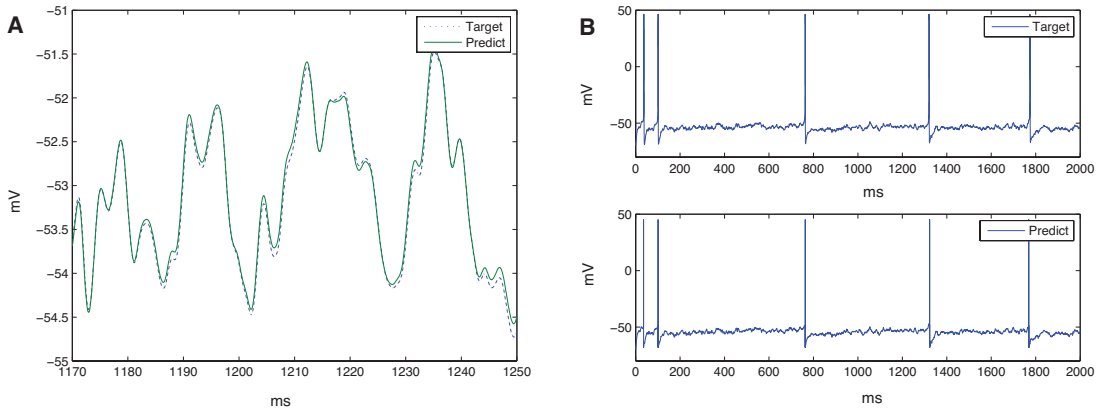


Figure 3.4: (A) Comparison of subthreshold dynamics. (B) Comparison of spike trains. Target data for both (A) and (B) is generated by white noise input to the detailed ion-channel based model [17] for a regular-spiking cortical cell.

racy of the prediction. While the reference data used presented 37 spikes during a $2s$ period of time, the prediction estimated an average 37.2 spikes, resulting in an over-prediction of only 0.2 spikes. During the validation process, the difference between the number of spikes in the target data, and the predicted ones differed at most by 3 spikes.

### 3.3.2 Experimental Data

For the experimental part of the research, primary cultures of embryonic rat motoneurons were prepared according to NIH guidelines and in agreement with the Institutional Animal Care and Use Committee (IACUC) approved protocol. Rat spinal motoneurons were dis-

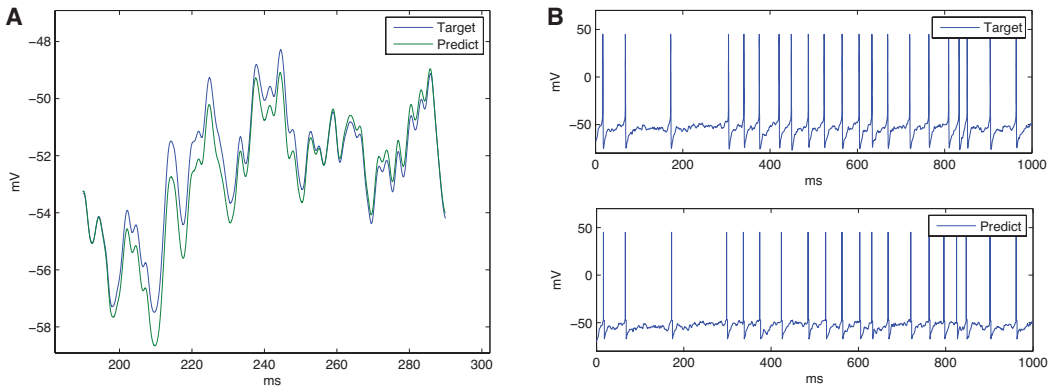


Figure 3.5: Target data generated from a detailed ion-channel based model for a fast-spiking cortical neuron [17]. (A) Target and predicted subthreshold dynamics. (B) Target v.s. predicted spike trains under noisy input.

sected from day 14 (E14) embryos as published earlier [40] . Cells were dissociated with trypsin (Invitrogen, 0.05%) and centrifuged for $15min$ at $500g$. Motoneurons were purified with immunopanning using antibodies (antibody 192, 1:2 dilution, ICN Biomedicals, Akron, OH) recognizing the low affinity NGF receptor expressed only by ventral motoneurons at this age. Purified motoneurons were plated on 22x22$mm^2$ ornithine/laminin coated coverslips at a density of 200 cells/$mm^2$ in Neurobasal (Gibco-BRL) medium supplemented with B27 (2% v/v; Invitrogen), L-glutamine (0.5 $mM$), 2-mercaptoethanol (25 $\mu M$), glial cell line-derived neurotrophic factor ($1ng/ml$ CNTF; Cell Sciences) L-glutamate (25 $\mu M$) was added to the culture medium during the first 5 days of growth.

Conventional whole-cell path clamp recordings were performed on the culture cells between day 7 and 14 in culture. The extracellular solution was Neurobasal culture medium,

the pH was adjusted to 7.3 with HEPES. Patch pipets were prepared from borosilicate glass (BF150-86-10; Sutter, Novato, CA) with a Sutter P97 pipet puller and filled with intracellular solution (in $mM$: K-gluconate 140, EGTA 1, MgC12 2, Na2ATP 2, phosphocreatine 5, phosphocreatine kinase 2.4 $mg$, Hepes 10; pH:7.2). The resistance of the electrodes was 6-8$M\Omega$. Current clamp experiments were performed with the Multiclamp 700A amplifier (Axon, Union City, CA). Signals were digitized at 10kHz with an Axon Digidata 1322A interface. Data recording and initial analysis were performed with pClamp 10 software (Axon). White noise current was injected in current clamp mode from stimulus files at resting membrane potential. The amplitude of the current signal was adjusted to evoke subthreshold and suprathreshold (action potential) responses from the cells. The experimental data contained noise which might be the result of the measurements, the environment, or a combination thereof. Therefore, before subjecting the data to the estimation algorithms, the noisy data was first run through a low-pass filter. Specifically, an $8^{th}$ order Butterworth low pass filter with a cut-off frequency of 600Hz was utilized. The filtered data was then processed to determine the location of spikes in the spike train. A sufficiently long piece of subthreshold data (*i.e.*, a data subsequence without any spikes) was also selected for Stage I of the proposed two-stage estimation strategy.

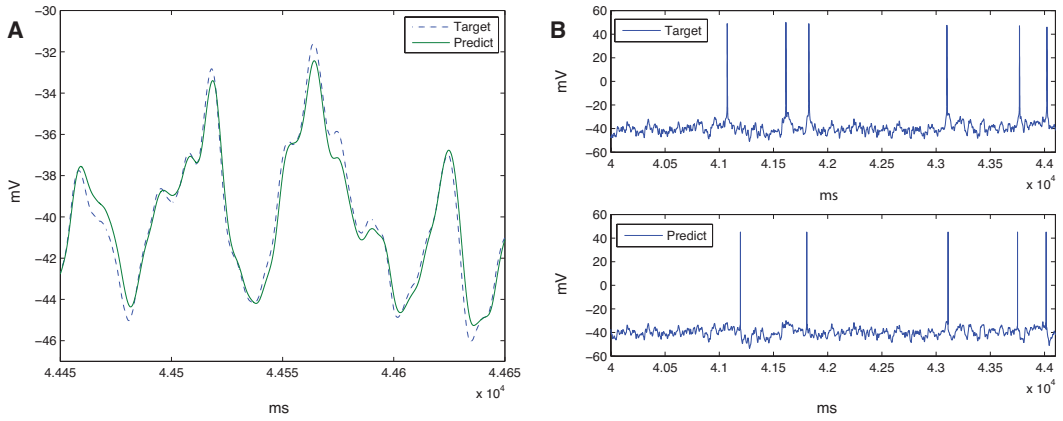


Figure 3.6: (A) Comparison of subthreshold dynamics. (B) Comparison of spike trains. Target data for both (A) and (B) is generated by white noise input injected into embryonic rat motoneurons.

#### 3.3.2.1 Experimental Results

As in the case of the detailed Hodgkin-Huxley model, the results presented here for evaluation use previously unseen data, *i.e.*, the data stream utilized for model evaluation is different from that utilized for generating the estimated model. Fig. 3.6A shows the subthreshold approximation using the estimated parameters from which it is clear to see that the linear model dynamics of (3.1) and (3.2) are a good approximation in the subthreshold regime. Fig. 3.6B shows a subsequence of the target and predicted spike trains, where the prediction misses one spike but locates the remaining spikes correctly. The statistics after 10 evaluations of the experimental data revealed that 16 spikes were predicted while the target data had 14 spikes, *i.e.*, the mean prediction error was 2 spikes.

# CHAPTER 4

# CONCLUSIONS

A weighted least squares approach to estimate parameters in a simple adaptive quadratic spiking neuron model has been proposed. It was shown that the discontinuity in the resetting can be cast as an impulse train in the system dynamics. By developing a linear-in-the-parameters model, a prediction error-based weighted least squares method was formulated that allows for estimation of model parameters through measurements of injected current and membrane potential only. Several tests were run to demonstrate the validity as well as robustness of this approach to noise. Preliminary results using data from a detailed ion channel based model suggest directions for further improvement. Future work will focus on adequately modeling detailed simulation and experimental data.

While the results for prediction of reference data generated from the quadratic model itself show good prediction and robustness under noise, the prediction of data obtained from the detailed ion-channel (*i.e.,* Hodgkin-Huxley type model) merits more discussion. Specifically, there are differences between data obtained from the detailed ion-channel model and the assumptions made by the quadratic model. For example, the downstroke of the action potential (*i.e.,* spike) in the detailed ion-channel based model is not a discontinuity as

assumed in the quadratic model; instead, the downstroke is akin to a downhill ramp which descends in about $2ms$ to its resting value in this model. In fact, the observations of the estimates suggests that the penultimate term in (2.13) is appropriate to model the upstroke of the spike whereas its intended purpose in the quadratic model is to capture the falling edge of the spike. Similarly, the final term in (2.13) is appropriated to model the downstroke of the spike whereas its intended purpose is to capture the adaptation in the model due to spike occurrence. This suggests the need to do one of the following: (1) to pre-process the output of the detailed model to replace the ramp like downstroke with a hard reset – this is acceptable because we are interested merely in replicating firing patterns and not action potential shapes, however, this requires *a priori* knowledge of the reset voltage. (2) to replace the hard reset term in (2.13) with a ramp like term, however, this would require an adjustment to suspend the original system dynamics during that interval. Moreover, in addition to utilization of weights to enforce good estimation of the behavior around the spike instants, hard bounds need to be enforced on estimates for those parameters that are known to be positive or negative in order to ensure better prediction, *e.g.,* the parameter encoding for reset after a spike should be upper-bounded by 0.

It should be noted that the exact spike time is highly sensitive to parameter estimation error, *i.e.,* the results suggest that a small error in parameter estimation might cause the prediction and the reference to be mismatched; however, the firing rate and patterns remain similar. Since mean firing rate carries information about experimental conditions and specific firing pattern may convey significant behavioral information [25] and, for large networks of

spiking neurons, the firing rate of each neuron in the network is a function of the firing rates of all the other neurons [26], it is much more important to replicate the rate of firing and the firing pattern. In any case, due to the inherent noise in an experimental environment, accurate parameter estimation is nearly impossible. Furthermore, it is more practical and useful to determine a distribution of the parameters since the experimental data under different conditions suggest that there is a stochastic variable in neuronal activity [14].

To overcome some of the issues of the proposed adaptive quadratic model, a stochastic resonate-and-fire model was studied. Based on evidence from empirical data and existing literature, the voltage threshold for the resonate-and-fire model was assumed to be random and normal. By formulating the estimation of parameters as a two-stage problem, an estimation mechanism based on nonlinear least squares subthreshold estimation and maximum likelihood spike pattern estimation was presented. The estimation mechanism was fed with simulated data as well as *in vitro* experimental data obtained from embryonic rat motoneurons to obtain results that corroborated the validity of the mechanism. The data used for parameter estimation was different from that used to validate the results given by the prediction resonate-and-fire model based on the estimated parameters. The simulation and experimental results presented show a very good match between the prediction and the target.

In the presented formulation, it was assumed that the subthreshold trace could be defined as a "linear zone" where the dynamics (3.1) and (3.2) are a good approximation. This subthreshold region is upper-bounded by the variable threshold. Results shown in the last

section indicate the validity of this assumption, since the error between the prediction and the target in Figs. 3.4, 3.5, and 3.6 is below 5%. Since the linear model is capable of replicating only the subthreshold dynamics, the reference voltage trace used for the nonlinear least squares estimation should not contain any spikes. This is ensured by choosing a sufficiently long data subsequence between spikes, with starting and ending points far away from the nearest spike. By sufficiently long subsequence, it is meant that the input output data should be long enough to lead to subthreshold parameter convergence – this is a standard assumption made in system identification. Furthermore, by ensuring that the starting point of the data is far away from a spike, one can ignore the transient artifacts related to the initial conditions (*i.e.,* reset) immediately following a spike.

Another assumption made in this formulation is that all the stochastic components in the system, including system noise (either caused by measurement noise or by the environment of the cell) as well as the variability of the threshold, can be captured by the threshold distribution that has been employed. Results suggest that such a simplification leads to a small over-prediction of the firing rate on average. However, the results are still acceptable - the errors are small in percentage and the predicted spike trains have remarkably similar spiking patterns as the targets that they are intended to emulate. A model with more sophisticated assumptions or additional components could most likely address the over-prediction issue, yet this would result in a larger computation cost.

Computation of the likelihood function (3.8) is the major cost of computation in the proposed two-stage estimation strategy. The original likelihood function is defined over

all time instants. The simulated data is sampled at 50kHz and the experimental data is sampled at 10kHz. This results in a large size of $\{t_i\}$ as defined in Section 3.2.2. In practice, considering the fact that $G(V_t; m, \sigma)$ is a Gaussian probability density function which is practically zero beyond $3\sigma$ distance from the mean $m$, the voltage trace is preprocessed to make $\{t_i\}$ only contain points that are not too far away from the mean. This requires some *a priori* knowledge about the parameters before we delve into the estimation. This is deemed acceptable since one can easily draw reasonable bounds for the parameters $m$ and $\sigma$ from an examination of the reference spike train.

# LIST OF REFERENCES


[1] L. Paninski, J. W. Pillow, E. P. Simoncelli, "Maximum Likelihood Estimation of a stochastic Integrate-and-Fire Neural Encoding Model, " Neural Computation, vol. 16, pp. 2533-2561, 2004.

[2] E. M. Izhikevich, "Simple Model of Spiking Neurons," *IEEE Trans. Neural networks,* vol. 14, pp. 1569-1572, Nov. 2003.

[3] A. N. Burkitt, "A Review of the Integrate-and-Fire Neuron Model: I. Homogeneous Synaptic Input," *Biological Cybernetics*, vol. 95, pp. 1-19, Apr. 2006.

[4] E. M. Izhikevich, "Which Model to Use for Cortical Spiking Neurons?" *IEEE Trans. Neural networks,* vol. 15, pp. 1063-1070, Sep. 2004.

[5] E. M. Izhikevich, *Dynamical Systems in Neuroscience: The Geometry of Excitability and Bursting*, The MIT Press, 2007.

[6] R. Naud, N. Marcille, C. Clopath, W. Gerstner, "Firing Patterns in The Adaptive Exponential Integrate-and-Fire Model," *Biological Cybernetics.* vol. 99, pp. 335-347, 2008.

[7] D. Haufler, F. Morin, J. C. Lacaille, F. K. Skinner, "Parameter Estimation in Single-compartment Neuron Models Using a Synchronization-based Method," *Neurocomputing*, vol. 70, pp. 1606-1610, 2007.

[8] R. Brette, W. Gerstner, "Adaptive Exponential Integrate-and-Fire Model as an Effective Description of Neuronal Activity," *J. Neurophysiol* vol. 94, pp. 3637-3642, Jul. 2005.

[9] G. LeMasson, R. Maex, *Introduction to Equation Solving and Parameter Fitting. In: Computational Neuroscience: Realistic modeling for Experimentalists.* London: CRC Press, 2001.

[10] M. C. Vanier, J. M. Bower, "A Comparative Survey of Automated Parameter-Search Methods for Compartmental Neural Models," *Journal of Computational Neuroscience*, vol. 7, pp. 149-171. 1999.

[11] A. A. Prinz, C. P. Billimoria, E. Marder, "Alternative to Hand-Tuning Conductance-Based Models: Construction and Analysis of Database of Model Neurons," *J. Neurophysiol* vol.90, pp. 3998-4015, Aug. 2003.

[12] Christina M. Weaver and Susan L. Wearne, "The Role of Action Potential Shape and Parameter Constraints in Optimization of Compartment Models," *Neurocomputing*, vol. 7, pp. 149-171, 1999.

[13] Ping Zhang and Jianfeng Feng, " Ideal Obvserver of Single Neuron Activity," *Neurocomputing*, vol. 44-46, pp. 243-247, 2002.

[14] P. Lansky, P. Sanda, J. He, "The Parameters of the Stochastic Leaky Integrate-and-Fire Neuronal Model," *J Comput Neurosci*, vol. 21, pp. 211-223, 2006.

[15] X. Zhang, G. You, T. Chen, and J. Feng, "Maximum Likelihood Decoding of Neuronal Inputs from Interspike Interval Distribution," *Neural Computation*, vol. 21, pp. 3079-3105, 2009.

[16] Jun Chen, Peter Molnar, Aman Behal, "A Weighted Least Squares Approach for Identification of a Reduced-Order Adaptive Neuronal Model," *Submitted to IEE Transactions on Neural Networks.*

[17] D. A. McCormick, Z. Wang, J. Huguenard, "Neurotransmitter Control of Neocortical Neuronal Activity and Excitability," *Cereb Cortex.* vol. 3, pp. 387-398. 1993.

[18] A. Destexhe, D. Contreras, M. Steriade, "Mechanisms Underlying the Synchronizing Action of Corticothalamic Feedback Through Inhibition of Thalamic Relay Cells," *J. Neurophysiol* vol. 79, pp. 999-1016, Feb. 1998.

[19] *http://senselab.med.yale.edu/senselab/modeldb/ShowModel.asp?model=3817*

[20] J. J. Slotine, W. Li, *Applied Nonlinear Control*, New York: Prentice Hall, 1991.

[21] M.L. Hines and N.T. Carnevale, "The NEURON simulation environment", *Neural Computat.* vol. 9, pp. 1179-1209, 1997.

[22] C. M. Gray, D. A. McCormick, "Chattering Cells Superficial Pyramidal Neurons Contributing to the Generation of Synchronous Oscillations in the Visual Cortex," *Science*, vol. 274, no. 5284, pp. 109-113, Oct. 1996.

[23] P. C. Young, C. J. Taylor, W. Tych, D. J. Pedregal, P. G. McKenna, "The Captain Toolbox," Centre for Research on Environmental Systems and Statistics, Lancaster University, 2004.

[24] H. Garnier, M. Gilson, "The CONTSID toolbox for Matlab," Centre de recherche en Automatique de Nancy (CRAN), Nancy-University, www.cran.uhp-nancy.fr/contsid, 2009

[25] H. Nakahara, S. Amari, "Information-Geometric Measure for Neural Spikes," *Neural Computation*, vol. 14, pp. 2269-2316, 2002.

[26] N. Brunel, P. E. Latham, "Firing Rate of the Noisy Quadratic Integrate-and-Fire Neuron," *Neural Computation*, vol. 15, pp. 2281-2306, 2003.

[27] A. Hodgkin, A. Huxley, "A Quantitative Description of Membrane Current and Its Application to Conduction and Excitation in Nerve, " *J. Physiol*, vol. 117, pp. 500-544, 1952.

[28] G. Young, "Note on Excitation Theory, " *Psychometrika*, vol. 2, no. 2, 1937.

[29] R. FitzHugh, "Mathematical Models of Excitation and Propagation in Nerve, " In H. P. Schwan, *Biological Engineering*. New York: McGraw-Hill.

[30] Eugene M. Izhikevich, "Resonate-and-fire Neurons," *Neural Networks*, vol. 14, pp 883-894, 2001.

[31] R. Jolivet, T. J. Lewis, W. Gerstner, "Generalized Integrate-and-Fire Models of Neuronal Activity Approximate Spike Trains of a Detailed Model to a High Degree of Accuracy," *J. Neurophysiol* vol. 92, pp. 959-976, 2004.

[32] R. Azouz, C. M. Gray., "Dynamic Spike Threshold Reveals a Mechanism for Synaptic Coincidence Detection in Cortical Neurons *in vivo*, " *Proc. Natl. Acad. Sci. USA*, vol. 97, pp. 8110-8115, 2000.

[33] Jun Chen, Jose Suarez, Peter Molnar, and Aman Behal, "Maximum Likelihood Parameter Estimation in a Stochastic Resonate-and-Fire Neuronal Model," *1st IEEE International Conference on Computational Advances in Bio and Medical Sciences*, Orlando, Fl, pp. 57-62, 2011.

[34] A. Bershadskii, E. Dremencov, G. Yadid, "Short-term Memory and Critical Clusterization in Brain Neurons Spike Series, " *Physics Letter A*, vol. 313, pp. 158-161, 2003

[35] John A. White, Ruby Klink, Angel Alonso, Alan R. Kay, "Noise From Voltage-Gated Ion Channels May Influence Neuronal Dynamics in the Entorhinal Cortex ," *J Neurophysiol*, vol. 80, pp. 262-269, 1998.

[36] Ian C. Bruce, Laurence S. Irlicht, "Renewal-Process Approximation of a Stochastic Threshold Model for Electrical Neural Stimulation ," *J Comput Neurosci*, vol. 9, pp. 211-223, 2000.

[37] C. T. Kelley, *Iterative Methods for Optimization*, SIAM Frontiers in Applied Mathematics, 1999

[38] S. Kirkpatrick, C. D. Gelatt, M. P. Vecchi, "Optimization by Simulated Annealing," *Science*, Vol. 220, No. 4598, pp. 671-680, 1983.

[39] A. Corana, M. Marchesi, C. Martini, S. Ridella, "Minimizing Multimodal Functions of Continuous Variables with the "Simulated Annealing" Alogrithm," *ACM Transactions on Mathematical Software*, vol. 13, No. 3, pp. 262-280, 1987.

[40] M. Das, P. Molnar, H. Devaraj, M. Poeta, J.J. Hickman, "Electrophysiological and Morphological Characterization of Rat Embryonic Motoneurons in a Defined System," *Biotechnol.* Prog. 19, pp. 1756 -1761, 2003.